Limit Cycle Minimization by Time-Invariant Extremum Seeking Control

Saurav Kumar[1,2], Alireza Mohammadi[4], Robert D. Gregg[2,3] and Nicholas Gans[5]

Abstract— **Conventional perturbation-based extremum seeking control (ESC) employs a slow *time-dependent* periodic signal to find an optimum of an unknown plant. To ensure stability of the overall system, the ESC parameters are selected such that there is sufficient time-scale separation between the plant and the ESC dynamics. This approach is suitable when the plant operates at a fixed time-scale. In case the plant slows down during operation, the time-scale separation can be violated. As a result, the stability and performance of the overall system can no longer be guaranteed. In this paper, we propose an ESC for periodic systems, where the external *time-dependent* dither signal in conventional ESC is replaced with the periodic signals present in the plant, thereby making ESC *time-invariant* in nature. The advantage of using a *state-based* dither is that it inherently contains the information about the rate of the rhythmic task under control. Thus, in addition to maintaining time-scale separation at different plant speeds, the adaptation speed of a time-invariant ESC automatically changes, without changing the ESC parameters. We illustrate the effectiveness of the proposed time-invariant ESC with a Van der Pol oscillator example and present a stability analysis using averaging and singular perturbation theory.**

I. INTRODUCTION

Limit cycles occur in numerous natural phenomena and engineering applications, e.g., human locomotion, turbines, etc., whose qualitative behaviors are often captured by simple oscillator models [1]. To optimize the performance of such systems in real-time, a conventional perturbation-based extremum seeking control (ESC) [2], [3] was used in [4], [5]. Conventional ESC schemes use a slow, exogenous *time-dependent* periodic signal such as $d(t) = a \sin \omega t$, known as the dither signal, to estimate the local gradient and optimize the steady-state objective of a plant with unknown dynamics. From hereon, we refer to such schemes as *time-based* ESC. The conventional stability analysis of time-based ESC requires sufficient time-scale separation between the plant and the ESC dynamics and inherently assumes that the plant operates at a fixed time-scale. Accordingly, the dither frequency, ω, is judiciously chosen small enough such that the ESC dynamics is at least an order of magnitude slower than the plant dynamics.

However, there are applications where the plant no longer operates at a fixed time-scale, and the speed of the plant dynamics varies with time. Human locomotion is an example of such system, which exhibits varying time-scales based on the activity (e.g., walking speed) [6], [7]. In a transfemoral powered prosthetic leg, the evolution of the knee and the ankle joints are typically synchronized to the human's hip signal [8], [9]. The hip signal is generated at a faster rate when the prosthetic leg user speeds up, thereby causing the prosthetic leg to operate faster. Similarly, when the user slows down, the rate of hip signal generation decreases and the prosthetic leg operates at a slower speed. For such systems, if the desired task results in slow operation speed, the time-scale separation between the plant and the ESC dynamics is violated and the conventional ESC structure can no longer be guaranteed to be stable.

Our objective is to use the conventional ESC structure for periodic plants with *varying time-scales* while ensuring stability, without the need for changing the dither signal parameters. To achieve this, we replace the time-dependent dither signal in conventional ESC with a function of the states of the periodic system. We call this ESC scheme using state-based dither as *time-invariant* ESC. The state-based dithers inherently contain information about the rate of the rhythmic task under control, as opposed to the conventional time-based dither signals that are external to the dynamical system. As a result, when the plant speed changes, the state-based dither parameters (e.g., frequency) automatically change, thus eliminating the need for manual tuning to maintain time-scale separation. The trade-off for removing the need for time-scale separation between the plant and the ESC dynamics in time-invariant ESC is that it needs a measurement of one of the periodic states of the system, which can be unactuated. No other state information or knowledge of the system is needed for our approach, unlike [10], where the authors assume explicit relation between the plant dynamics and the unknown parameters and use estimation techniques to achieve extremum seeking.

To the best of our knowledge, no one has explored the use of periodic plant signals to generate ESC dithers. The closest works that avoid injecting a dither signal use external disturbances/noise to generate probing signals [11]–[14]. In [11], [12], a novel extremum seeking control algorithm was presented, which used atmospheric disturbances as the dither signal. In [13], [14], the dither signal of a time-based ESC was replaced with noise disturbances in the plasma control system for optimizing the performance of the Frascati Tokomak Upgrade. Both these works ensured that the dither

[1]Department of Electrical Engineering, [2]Department of Bioengineering, [3]Department of Mechanical Engineering, University of Texas at Dallas, Richardson, TX 75080, USA. [4]Department of Electrical and Computer Engineering, University of Michigan - Dearborn, USA. [5]UT Arlington Research Institute, University of Texas at Arlington. {sauravk,alireza.mohammadi,rgregg}@ieee.org, ngans@uta.edu

signal was sufficiently slower than the plant dynamics. There is also notable work to employ ESC approaches specifically tailored for systems with slow dynamics [15], [16].

Although the time-invariant ESC is applicable for general periodic systems, we used a Van der Pol oscillator as an example to illustrate the effectiveness of the proposed approach, similar to [4]. In particular, the periodic state of the Van der Pol oscillator was used as a state-based dither in time-invariant ESC to reduce the size of the limit cycle. We present a stability analysis of the overall system by averaging and singular perturbation methods. The simulation results show that the time-invariant ESC works across various speeds of plant dynamics without the need of changing the dither signal parameters. On the other hand, the time-based ESC with fixed dither signal parameters introduces large undesirable oscillations for slower plant dynamics.

The rest of the paper is organized as follows. In Section II, we present the model of a controlled Van der Pol oscillator and a brief review of a conventional time-based ESC. Next, we explain the structure of the time-invariant ESC and present the stability analysis in Section III. In Section IV, we present the simulation results of the proposed time-invariant ESC implemented on a Van der Pol oscillator and compare its performance with a time-based ESC. Section V concludes this paper.

II. PRELIMINARIES

In this section, we briefly review the equations of the Van der Pol oscillator and the time-based ESC scheme used in [4] for limit cycle minimization.

A. Van der Pol Oscillator

Consider the controlled Van der Pol oscillator described by [17]

$$\dot{x}_1 = x_2, \tag{1}$$
$$\dot{x}_2 = \varepsilon(1-(x_1-x_0)^2)x_2 - \mu^2(x_1-x_0) + u, \tag{2}$$
$$y = x_1 - x_0, \tag{3}$$

where $x_0 \in \mathbb{R}$ is an offset parameter of x_1. Assume that there exists a state feedback control law parameterized by $\theta \in \mathbb{R}$:

$$u = \alpha(x,\theta) := \varepsilon(\theta - \theta^*)^2 x_2, \tag{4}$$

where $\theta - \theta^*$ is a parameter that controls the amplitude and the frequency of oscillation of the states. $\theta^* \in \mathbb{R}$ represents the optimum θ, at which the amplitude of the limit cycle is minimum. The parameter $\varepsilon \in \mathbb{R}_+$ is a small parameter[1] that controls the speed of limit cycle transients, and $\mu \in \mathbb{R}_+$ controls the speed of limit cycle oscillations. Setting $\mu^2 = 1 - \varepsilon\bar{\mu}^2$, it can be seen that for $\varepsilon = 0$, and $x_1(0) = x_2(0) = r \neq 0$, the system (1)-(4) has a limit cycle with radius r. Therefore, it is natural for the Van der Pol oscillator to satisfy [4], [17]:

Assumption 2.1: *For small $\varepsilon > 0$, and for any θ, θ^*, the system* (1)-(4) *has a limit cycle with a radius $r > 0$.*

[1]The smallness of ε is needed to apply averaging tools to our problem, under which the study of limit cycle dynamics is reduced to the study of equilibrium dynamics.
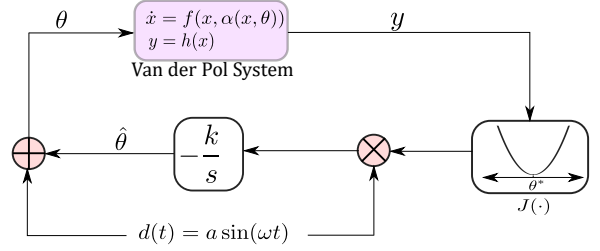

Fig. 1: Block diagram of a first order *time-based* ESC. In time-based ESC, the dither signal $d(t) = a\sin(\omega t)$ is an external time-dependent signal.

B. Conventional Time-Based ESC for Periodic Systems

Consider a single-input single-output nonlinear system

$$\dot{x} = f(x,u), \tag{5}$$
$$y = h(x), \tag{6}$$

where $x \in \mathbb{R}^n$ is the state vector with $n \geq 2$, $y \in \mathbb{R}$ is the output, and the functions $f : \mathbb{R}^n \times \mathbb{R} \to \mathbb{R}^n$ and $h : \mathbb{R}^n \to \mathbb{R}$ are smooth. Given the state feedback control law $u = \alpha(x,\theta)$, parameterized by a tunable parameter θ, the closed-loop control system dynamics are given by

$$\dot{x} = f(x,\alpha(x,\theta)). \tag{7}$$

The objective of ESC is to maximize/minimize, in real-time, a suitably defined objective function $J(\cdot)$ for the closed-loop dynamics trajectories without knowing *a priori* the extremum θ^* of the objective function $J(\cdot)$.

A well-known extremum seeking algorithm [2], [3], [18], [19] is the perturbation-based ESC, whose basic architecture is depicted in Fig. 1. The signal

$$d(t) = a\sin(\omega t), \tag{8}$$

is a periodic *time-dependent* perturbation signal that is added to the current best estimate of the parameter θ, i.e., $\hat{\theta}$. Taking θ as input, the system generates an output y, which is then used to compute the objective function $J(\cdot)$.

In [4], a time-based ESC was used to minimize the limit cycle amplitude. The limit cycle amplitude was computed by passing the output of the Van der Pol oscillator (see equation (3)) through an "amplitude detector", which was a combination of high-pass filtering, squaring, and low-pass filtering operations. The output of the amplitude detector was then used as an objective function $J(\cdot)$ by the ESC scheme. In the extremum seeking literature [3], [4], [18], [19] the following assumptions are typically made regarding the convex objective function:

Assumption 2.2: *There exists a unique optimum θ^*, such that*

$$J'(\theta^*) = 0, \quad J''(\theta^*) > 0, \tag{9}$$

where $J' = \frac{\partial J}{\partial \theta}$ and $J'' = \frac{\partial^2 J}{\partial \theta^2}$.

This assumption implies that the extremum of the objective function is a minimum. Without loss of generality, the extremum of the objective function can be a maximum by assuming $J''(\theta^*) < 0$ in (9). The goal of time-based ESC is to minimize the objective function $J(\cdot)$, satisfying Assumption
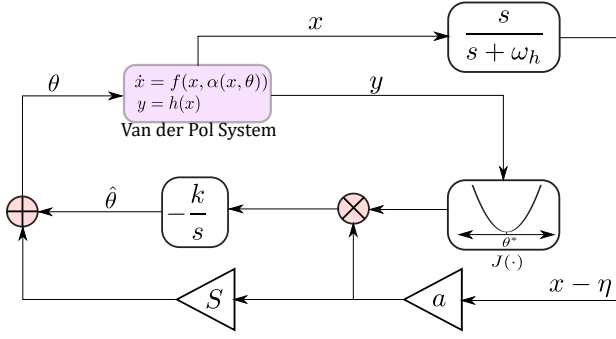
Fig. 2: Block diagram of a *time-invariant* ESC. The periodic state x_1 is passed through a high-pass filter, which generates a *time-invariant* dither signal.

2.2, by tuning θ. The output of the objective function block is then demodulated by using the same *time-dependent* dither signal $d(t)$. The resulting demodulated signal is then passed through an integrator with gain k to give $\hat{\theta}$. The sign of the integrator gain k should be chosen such that the inequality $kJ'' > 0$ holds.

Considering a first order ESC [18], its dynamics can be written as

$$\dot{\hat{\theta}} = -kaJ(\hat{\theta} + a\sin\omega t)\sin\omega t. \tag{10}$$

The choice of ESC parameters a, ω, $k \in \mathbb{R}_+$ are critical to stable adaptation and are normally chosen to be small to guarantee that a sufficient time-scale separation between the plant and the ESC dynamics holds. For the case of the Van der Pol oscillator, this means that the limit cycle oscillation frequency should be much faster than the dither frequency ω [4]. Denoting $\tilde{\theta} = \hat{\theta} - \theta^*$, the closed-loop dynamics of the Van der Pol oscillator (1)-(4) along with the time-based ESC dynamics (10) can be written as

$$\dot{x}_1 = x_2, \tag{11}$$
$$\dot{x}_2 = \varepsilon(1 - (x_1 \text{-} x_0)^2 + (\tilde{\theta} + a\sin\omega t)^2)x_2 - \mu^2(x_1 \text{-} x_0), \tag{12}$$
$$\dot{\tilde{\theta}} = -kaJ(\tilde{\theta} + \theta^* + a\sin\omega t)\sin\omega t. \tag{13}$$

The stability of the system (11)-(13) can be proved by following the steps in [4], which uses averaging and singular perturbation tools. Additional details regarding time-based ESC for optimizing the steady-state of a Van der Pol oscillator can be found in [4].

III. TIME-INVARIANT ESC

In this section, we first present the structure of time-invariant ESC. Next, we present the stability analysis of the closed-loop dynamics of the Van der Pol oscillator and time-invariant ESC using averaging and singular perturbation theory.

A. Structure of Time-Invariant ESC

Fig. 2 shows the block diagram of time-invariant ESC. Consider a general periodic system described by (5)-(6). In time-invariant ESC, we use a function of the periodic state of the system as a dither instead of a time-dependent dither such as $d(t) = a\sin\omega t$. In this work, we use the periodic state x_1, passing it through a high-pass filter (HPF) to remove the

DC component so that it satisfies the zero mean property of the dither signal. The output of the HPF is then scaled by a small gain $a \in \mathbb{R}_+$ to obtain the *state-dependent dither signal*

$$d(x) = a(x_1 - \eta), \tag{14}$$

where $x_1 - \eta$ is the output of the HPF. Similar to time-based ESC, the state-based dither, $d(x)$, is then multiplied with the objective function $J(\cdot)$ (which satisfies Assumption 2.2) to produce a gradient estimate of the objective J with respect to the input θ. The gradient estimate is then integrated with an integrator gain k to give the estimate of the input, $\hat{\theta}$. The state-based dither in (14) is then scaled and added to $\hat{\theta}$ according to

$$\theta = \hat{\theta} + Sa(x_1 - \eta), \tag{15}$$

where S is a positive constant scalar greater than a that is used to speed up the adaptation rate. The parameters S, a should be selected such that $Sa \ll 1$. The dynamics of the time-invariant ESC can be written as

$$\dot{\eta} = \omega_h(x_1 - \eta), \tag{16}$$
$$\dot{\hat{\theta}} = -kaJ(\hat{\theta} + Sa(x_1 - \eta)) \cdot (x_1 - \eta). \tag{17}$$

Thus, there are four tunable parameters for our proposed time-invariant ESC, i.e., a, k, S, and ω_h. Similar to the time-based ESC, the sign of k should be chosen such that the inequality $kJ'' > 0$ holds. It is remarked that we need only one of the periodic states of the system, e.g., x_1, to construct the dither signal.

For the case of Van der Pol oscillator (1)-(4), the periodic state x_1 is centered around x_0, which is removed by the HPF. The closed-loop dynamics of the Van der Pol oscillator (1)-(4) along with the time-invariant ESC (16)-(17) can be written as

$$\dot{x}_1 = x_2 \tag{18}$$
$$\dot{x}_2 = \varepsilon(1 \text{-} (x_1 \text{-} x_0)^2 + (\hat{\theta} \text{-} \theta^* + Sa(x_1 - \eta))^2)x_2 - \mu^2(x_1 \text{-} x_0) \tag{19}$$
$$\dot{\eta} = \omega_h(x_1 - \eta) \tag{20}$$
$$\dot{\hat{\theta}} = -kaJ(\hat{\theta} + Sa(x_1 - \eta)) \cdot (x_1 - \eta). \tag{21}$$

B. Stability Analysis

In this section, we prove the stability of the closed-loop dynamics, given by Equations (18)-(21).

Proposition 1: *Consider the dynamics given by* (18)-(21). *Let* $\mu^2 = 1 - \varepsilon\bar{\mu}^2$, $r(t) = \sqrt{x_1^2(t) + x_2^2(t)}$, *and* $\tan(t + \phi(t)) = -x_2(t)/x_1(t)$. *Then, the overall system dynamics can be written as*

$$\dot{r} = \varepsilon h(r, \eta, \tilde{\theta})\sin(t + \phi), \tag{22}$$
$$\dot{\phi} = \varepsilon \frac{h(r, \eta, \tilde{\theta})}{r}\cos(t + \phi), \tag{23}$$
$$\dot{\eta} = \varepsilon\alpha\omega_H'(r\cos(t + \phi) - \eta), \tag{24}$$
$$\dot{\tilde{\theta}} = -\varepsilon\alpha K'aJ(\tilde{\theta} + \theta^* + Sa(r\cos(t + \phi) - \eta))(r\cos(t + \phi) - \eta), \tag{25}$$

where

$$h(r, \eta, \tilde{\theta}) = r\sin(t + \phi) + r(\tilde{\theta} + Sa(r\cos(t + \phi) - \eta))^2\sin(t + \phi) - r^3\cos^2(t + \phi)\sin(t + \phi) - \bar{\mu}^2 r\cos(t + \phi). \tag{26}$$

Proof: To simplify the analysis, we consider $x_0 = 0$. Let $\mu^2 = 1 - \varepsilon\bar{\mu}^2$. The closed-loop dynamics (18)-(21) can be written as

$$\dot{x}_1 = x_2, \tag{27}$$

$$\dot{x}_2 = -x_1 - \varepsilon h(x_1, x_2, \eta, \tilde{\theta}), \tag{28}$$

$$\dot{\eta} = \omega_h(x_1 - \eta), \tag{29}$$

$$\dot{\tilde{\theta}} = -kaJ(\tilde{\theta} + \theta^* + Sa(x_1 - \eta)) \cdot (x_1 - \eta), \tag{30}$$

where

$$h(x_1, x_2, \eta, \tilde{\theta}) = (x_1^2 - 1 - (\tilde{\theta} + Sa(x_1 - \eta))^2)x_2 - \bar{\mu}^2 x_1. \tag{31}$$

When $\varepsilon = 0$, the solutions of (27), (28) are $x_1(t) = r\cos(t + \phi)$, $x_2(t) = -r\sin(t + \phi)$ where r, ϕ are constant. When $\varepsilon \neq 0$, we should expect a slow drift of r and ϕ. Similar to [20], [21], the evolution equations for r and ϕ that depends on the nonlinear term $h(x_1, x_2, \eta, \tilde{\theta})$ can be derived. Assuming that ε is small, the states of the Van der Pol oscillator will be nearly sinusoidal and have a period 2π approximately. Therefore, let

$$x_1(t) = r(t)\cos(t + \phi(t)), \tag{32}$$

$$x_2(t) = -r(t)\sin(t + \phi(t)), \tag{33}$$

where $r(t) = \sqrt{x_1^2(t) + x_2^2(t)}$ and $\tan(t + \phi(t)) = -x_2(t)/x_1(t)$. Now, let $\omega_h = \varepsilon\alpha\omega'_H$ and $k = \varepsilon\alpha K'$, where $\omega'_H > 0$ and $\alpha > 0$ is a small constant. K' has the same sign as k, which is selected such that it satisfies the inequality $kJ'' > 0$. By Assumption 2.2, $K' > 0$. Taking the derivative of $r(t)$ and $\tan(t + \phi(t))$ with respect to t, and substituting x_1, x_2 from equation (32), (33) in the equations for $\dot{r}$, $\dot{\phi}$, the proposition is proved. ∎

We now bring the dynamics in (22)-(25) into the standard averaging form. Treating $z = [r \ \phi \ \eta \ \tilde{\theta}]^T$, equations (22)-(25) can be represented in the succinct form as

$$\dot{z} = \varepsilon g(t, z, \varepsilon), \tag{34}$$

which is in the standard averaging form [17, Chapter 10] and thus, averaging theory can be applied. Given a function $g(t, z, \varepsilon)$, which is 2π-periodic in t and $\varepsilon > 0$, we can associate with (34) an autonomous average system

$$\dot{z} = \varepsilon\bar{g}(z) \tag{35}$$

where

$$\bar{g}(z) = \frac{1}{2\pi}\int_0^{2\pi} g(s, z, 0)ds. \tag{36}$$

Substituting the averaged state $\bar{z} = [\bar{r} \ \bar{\phi} \ \bar{\eta} \ \bar{\tilde{\theta}}]^T$ in (36) introduces an $O(\varepsilon^2)$ error. The averaged dynamics for equations (22)-(25) is computed as

$$\dot{\bar{r}} = \frac{\varepsilon}{2\pi}\int_0^{2\pi} h\sin(t + \bar{\phi})dt + O(\varepsilon^2), \tag{37}$$

$$\dot{\bar{\phi}} = \frac{\varepsilon}{2\pi}\int_0^{2\pi} \frac{h\cos(t + \bar{\phi})}{\bar{r}}dt + O(\varepsilon^2), \tag{38}$$

$$\dot{\bar{\eta}} = \frac{\varepsilon}{2\pi}\int_0^{2\pi} \alpha\omega'_H(\bar{r}\cos(t + \bar{\phi}) - \bar{\eta})dt + O(\varepsilon^2), \tag{39}$$

$$\dot{\bar{\tilde{\theta}}} = \frac{-\varepsilon}{2\pi}\int_0^{2\pi} \alpha K'aJ(\bar{\tilde{\theta}} + \theta^* + Sa(\bar{r}\cos(t + \bar{\phi}) - \bar{\eta})) \cdot (\bar{r}\cos(t + \bar{\phi}) - \bar{\eta})dt + O(\varepsilon^2). \tag{40}$$

Let $t + \bar{\phi} = \varphi$. Equation (26) at $\phi = \bar{\phi}$ can be rewritten as

$$h = r\sin\varphi + r(\tilde{\theta} + Sa(r\cos\varphi - \eta))^2\sin\varphi - r^3\cos^2\varphi\sin\varphi - \bar{\mu}^2 r\cos\varphi. \tag{41}$$

The first-order Taylor series expansion of $J(\cdot)$ at $\bar{\tilde{\theta}} + \theta^*$ is

$$J(\cdot) = J(\bar{\tilde{\theta}} + \theta^*) + J'(\bar{\tilde{\theta}} + \theta^*) \cdot (Sa(\bar{r}\cos(t + \bar{\phi}) - \bar{\eta})). \tag{42}$$

By substituting h from (41) in (37), (38) and $J(\cdot)$ from (42) in (40), the averaged dynamics (37)-(40) can be written as

$$\dot{\bar{r}} = \varepsilon\left(\frac{\bar{r}}{2}\left(1 + \bar{\tilde{\theta}}^2 + S^2a^2\bar{\eta}^2 - 2\bar{\tilde{\theta}}Sa\bar{\eta}\right) + \frac{\bar{r}^3}{8}\left(S^2a^2 - 1\right)\right) + O(\varepsilon^2), \tag{43}$$

$$\dot{\bar{\phi}} = -\frac{\varepsilon\bar{\mu}^2}{2} + O(\varepsilon^2) = \frac{\mu^2 - 1}{2} + O(\varepsilon^2), \tag{44}$$

$$\dot{\bar{\eta}} = -\varepsilon\alpha\omega'_H\bar{\eta} + O(\varepsilon^2), \tag{45}$$

$$\dot{\bar{\tilde{\theta}}} = \varepsilon\alpha\left(K'aJ\bar{\eta} - \frac{SK'a^2J'\bar{r}^2}{2} - SK'a^2J'\bar{\eta}^2\right) + O(\varepsilon^2). \tag{46}$$

Note that the state $\bar{\phi}$ does not appear in the dynamics of $\bar{r}$, $\bar{\eta}$, $\bar{\tilde{\theta}}$, and is independent of the other states. From (44), it can be seen that the phase increases linearly with time, with its rate of change depending on μ.

Proposition 2: Consider the dynamics given by (43)-(46). In the quasi-steady state, we have

$$\bar{r} = 2\sqrt{\left(\frac{1 + (\bar{\tilde{\theta}} - Sa\bar{\eta})^2}{1 - S^2a^2}\right)}, \tag{47}$$

$$\frac{d\bar{\eta}_r}{d\tau} = -\varepsilon\omega'_H\bar{\eta}_r, \tag{48}$$

$$\frac{d\bar{\tilde{\theta}}_r}{d\tau} = \varepsilon\left(K'aJ\bar{\eta}_r - 2SK'a^2J'\frac{(1 + (\bar{\tilde{\theta}}_r - Sa\bar{\eta}_r)^2)}{1 - S^2a^2} - SK'a^2J'\bar{\eta}_r^2\right). \tag{49}$$

Proof: Neglecting $O(\varepsilon^2)$ in (43)-(46) and defining a slow time-scale $\tau = \alpha t$, we express (43), (45), and (46) in τ time-scale as

$$\alpha\frac{d\bar{r}}{d\tau} = \varepsilon\left(\frac{\bar{r}}{2}\left(1 + (\bar{\tilde{\theta}} - Sa\bar{\eta})^2\right) + \frac{\bar{r}^3}{8}\left(S^2a^2 - 1\right)\right), \tag{50}$$

$$\frac{d\bar{\eta}}{d\tau} = -\varepsilon\omega'_H\bar{\eta}, \tag{51}$$

$$\frac{d\bar{\tilde{\theta}}}{d\tau} = \varepsilon\left(K'aJ\bar{\eta} - \frac{SK'a^2J'\bar{r}^2}{2} - SK'a^2J'\bar{\eta}^2\right), \tag{52}$$

which is in a standard singular perturbation form. The fast system is represented by (50), and the slow system is represented by (51)-(52). Setting $\alpha = 0$ in (50) and solving for $\bar{r}$ proves (47). Freezing $\bar{r}$ at its quasi-steady-state obtained in (47) and substituting it in (51)-(52) proves (48)-(49). ∎

Remark 1: *It can be seen from (47) that when $(\bar{\tilde{\theta}} - Sa\bar{\eta}) \to 0$ and $S^2a^2 \ll 1$, the radius of the Van der Pol oscillator converges to 2, which is in accordance with [17, Example 10.11].* Having derived the quasi-steady state dynamics in Proposition 2, we now determine the equilibrium point $[\bar{\eta}_r^e \ \bar{\tilde{\theta}}_r^e]^T$ of the reduced averaged system, which

satisfies

$$\bar{\eta}_r^e = 0, \tag{53}$$

$$K'aJ'\bar{\eta}_r^e - 2SK'a^2J'\frac{(1+(\bar{\bar{\theta}}_r^e - Sa\bar{\eta}_r^e)^2)}{1-S^2a^2} - SK'a^2J'\bar{\eta}_r^{e2} = 0. \tag{54}$$

Note that the term

$$\frac{(1+(\bar{\bar{\theta}}_r^e - Sa\bar{\eta}_r^e)^2)}{1-S^2a^2} \neq 0. \tag{55}$$

Otherwise, $\bar{\bar{\theta}}_r^e$ is imaginary, which is not possible, and $\bar{r} = 0$ in equation (47), which violates Assumption 2.1. This implies that, based on Assumption 2.2,

$$J'(\bar{\bar{\theta}}_r^e + \theta^*) = 0 \iff \bar{\bar{\theta}}_r^e = 0. \tag{56}$$

Thus, the equilibrium point of the reduced averaged system (48)-(49) is $\bar{\eta}_r^e = \bar{\bar{\theta}}_r^e = 0$.

Theorem 1: Suppose that $\varepsilon, S, K', a > 0, S^2a^2 \ll 1$. Under Assumption 2.2, the reduced averaged system (48)-(49) is locally exponentially stable.

Proof: The Jacobian A_r of (48)-(49) at $[\bar{\eta}_r^e \ \bar{\bar{\theta}}_r^e]^T$ is

$$A_r|_{\bar{\eta}_r^e = \bar{\bar{\theta}}_r^e = 0} = \begin{bmatrix} -\varepsilon\omega_H' & 0 \\ 0 & -\varepsilon\frac{2SK'a^2}{1-S^2a^2}J''(\theta^*) \end{bmatrix}. \tag{57}$$

Since A_r is a diagonal matrix, we know that A_r will be Hurwitz if and only if

$$\varepsilon\frac{2SK'a^2}{1-S^2a^2}J''(\theta^*) > 0. \tag{58}$$

Based on our assumptions that the constants $\varepsilon, S, K', a > 0$, $S^2a^2 \ll 1$, and $J''(\theta^*) > 0$ (see Assumption 2.2) we can see that equation (58) is satisfied. Similarly, if J is strictly concave, we know that $J''(\theta^*) < 0$ and equation (58) can be satisfied by selecting $K' < 0$. This concludes the proof. ∎

Next, we analyze the boundary layer model to complete the singular perturbation analysis.

Theorem 2: *Consider the singularly perturbed system (50)-(52). There exists $\alpha^* > 0$ such that $\forall \ \alpha \in (0, \alpha^*)$, the equilibrium point of (50)-(52) is locally exponentially stable.*
Proof: The boundary layer model (in the $t = \tau/\alpha$ time-scale) is given by

$$\frac{d\bar{r}_b}{dt} = \varepsilon\left(\left(\bar{r}_b + 2\sqrt{\frac{1+\theta^2}{1-S^2a^2}}\right)\left(\frac{1+\theta^2}{2}\right) - \left(\frac{1-S^2a^2}{8}\right)\left(\bar{r}_b + 2\sqrt{\frac{1+\theta^2}{1-S^2a^2}}\right)^3\right). \tag{59}$$

By taking the Jacobian of (59), it can be easily shown that the equilibrium point $\bar{r}_b^e = 0$ of the boundary-layer model (59) is locally exponentially stable. Since the equilibrium point $[\bar{\eta}_r^e \ \bar{\bar{\theta}}_r^e]^T$ of the reduced averaged system (48)-(49) and the equilibrium point $\bar{r}_b^e$ of the averaged boundary layer model (59) are locally exponentially stable, by [17, Theorem 11.4] concludes the proof. ∎

Remark 2: *In our derivations for the time-invariant ESC, the small parameter ε is used to make the averaging analysis*

feasible. Furthermore, the parameter α was employed to bring the system into a singular perturbation form. We remark that α is not a system parameter and therefore, when the frequency of operation of the Van der Pol oscillator changes based on μ, the time-scale separation in (50)-(52) will not be affected. However, in [4], $1/\mu$ was taken as a small parameter in order to obtain the averaged system. As μ decreases, $1/\mu$ is no longer small, and averaging cannot be applied in that approach.
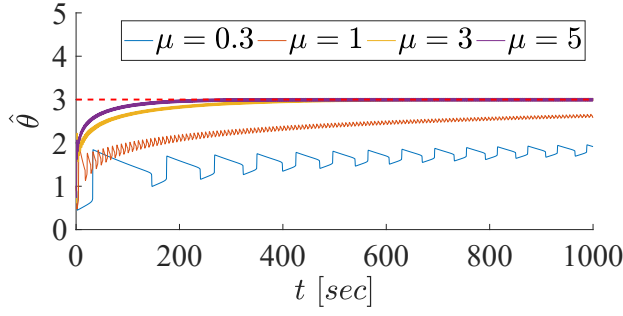
IV. SIMULATION RESULTS

The closed loop dynamics of the Van der Pol oscillator and the time-invariant ESC, represented by equations (18)-(21) were simulated. The initial conditions were chosen to be $x_1(0) = 4.5$, $x_2(0) = 0$, $\eta(0) = 0$, $\hat{\theta}(0) = 1$. The parameters of the Van der Pol oscillator were set to $x_0 = 6$, $\varepsilon = 1$, $\theta^* = 3$. The parameters of the time-invariant ESC were set to $a = 0.01$, $k = 10$, $S = 15$, and $\omega_h = 10$ rad/s. Similar to [4], we chose the objective function $J = y^2 = (x_1 - x_0)^2$. We ran simulations for $\mu = 0.3$, 1, 3, and 5, which corresponded to slow, normal, fast and very fast oscillations of the Van der Pol system.
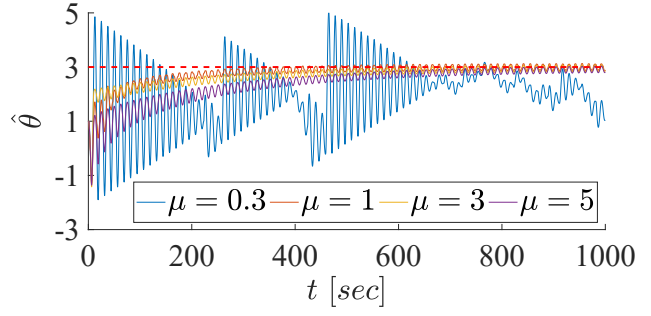
In order to compare the performance of time-invariant ESC with a time-based ESC, we tuned the parameters of the time-based ESC such that they work across different values of μ. In particular, the parameters $a = 0.01$, $k = 6$, and $\omega = 0.5$ rad/s were selected for the time-based ESC. Fig. 3 shows a performance comparison between the time-invariant and time-based ESC.

Figs. 3a, 3b show time-invariant and time-based ESC adaptation of $\hat{\theta}$ for different values of μ, respectively. It can be noticed from Fig. 3a that the adaptation speed increases for higher μ without changing the time-invariant ESC parameters. Fig. 3b shows that the time-based ESC adaptation produces severe oscillations in $\hat{\theta}$ for $\mu = 0.3$. This is because at $\mu = 0.3$, the Van der Pol oscillator slows down, and the time-scale separation between the plant and the ESC dynamics is violated. The convergence rate of the time-invariant ESC slows down as μ decreases and requires about 60000 seconds to converge for $\mu = 0.3$. In the time-based ESC, this trade-off between the convergence speed and stability also exists, but the control designer has to explicitly deal with it through the choice of the ESC parameters [18].
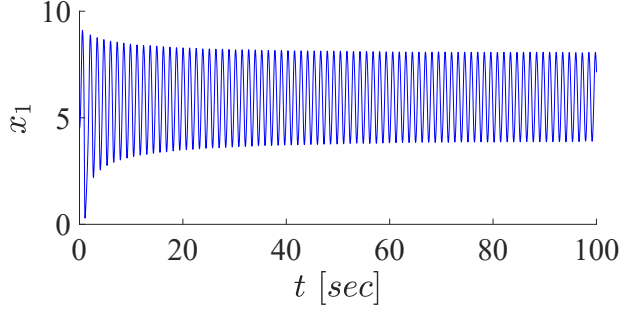
Fig. 3c shows the plot of the state x_1 with time-invariant ESC at $\mu = 5$. It can be seen that the magnitude of x_1 decreases over time, and there is no apparent oscillation in magnitude. From Fig. 3d it can be seen that the magnitude of x_1 had undesirable oscillations due to the time-based dither. In order to reduce the effect of the dither signal on the state x_1, the parameters of the time-based ESC need to be re-tuned. As noted by the authors in [18], the stability and the performance of a time-based ESC relies on the selection of proper parameters, which can be difficult to tune due to the dependence of one parameter on the other. Based on our experience, the parameters of a time-invariant ESC are much easier to tune than a time-based ESC.
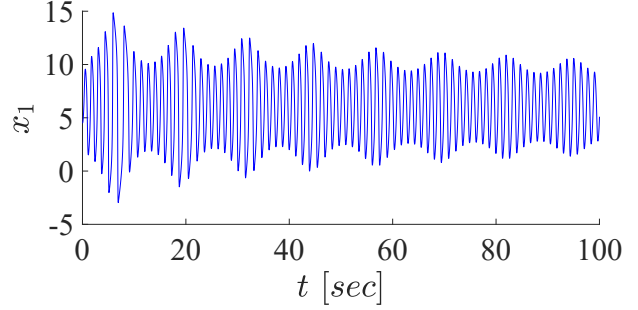
(a) Time-invariant ESC adaptation of θ for different values of μ.

(b) Time-based ESC adaptation of θ for different values of μ.

(c) Plot of x_1 with time-invariant ESC for μ=5.

(d) Plot of x_1 with time-based ESC for μ=5.

Fig. 3: Performance comparison between time-based and time-invariant ESC. Figs. 3a, 3b shows the time-based and time-invariant ESC adaptation of θ to $\theta^* = 3$ for different values of μ without changing the ESC parameters. Figs. 3c, 3d shows the periodic state x_1 of the Van der Pol oscillator with the time-based and time-invariant ESC for $\mu = 5$. It can be seen that although the time-based ESC is stable for $\mu = 5$, it introduces additional oscillations in the state x_1.
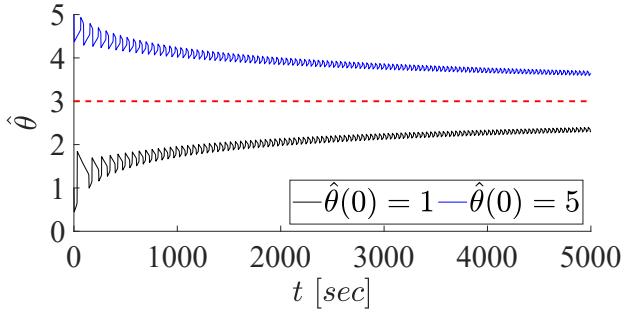

Fig. 4: Time-invariant ESC adaptation of $\hat{\theta}$ with $\mu = 0.3$ from different initial conditions of $\hat{\theta}$.
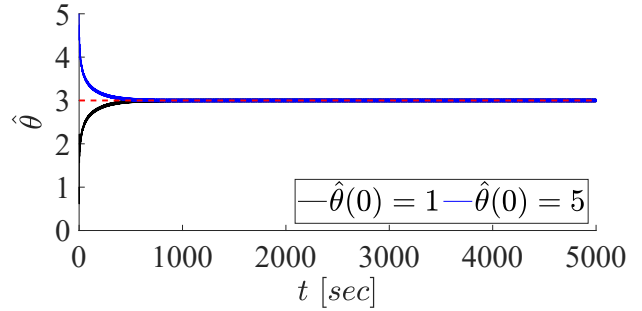

Fig. 5: Time-invariant ESC adaptation of $\hat{\theta}$ with $\mu = 3$ from different initial conditions of $\hat{\theta}$.

In order to show the efficacy of time-invariant ESC for small values of μ, Fig. 4 shows the plot of $\hat{\theta}$ starting from both the sides of the optimum, i.e., $\hat{\theta}(0) = 1$ and $\hat{\theta}(0) = 5$ for $\mu = 0.3$. Fig. 5 shows the plot of $\hat{\theta}$ with a time-invariant ESC scheme at $\mu = 3$ using the same parameters. From Figs. 4, 5, the difference in adaptation speed for different values of μ can be clearly seen. Figs. 6, 7 show the state-based dither signal for $\mu = 0.3$ and $\mu = 3$, respectively. By comparing the initial and the final 200 seconds of simulations in Figs. 6, 7, it can be seen that the time-invariant dither amplitude decreases, and its frequency increases with time[2]. Also, by comparing the dither signals for different values of μ, it can be noticed from Figs. 6, 7 that the amplitude and the

[2]The change in the dither frequency with time for $\mu = 3$ can be noted by comparing the number of troughs that appear on the magnified plots in Fig. 7.
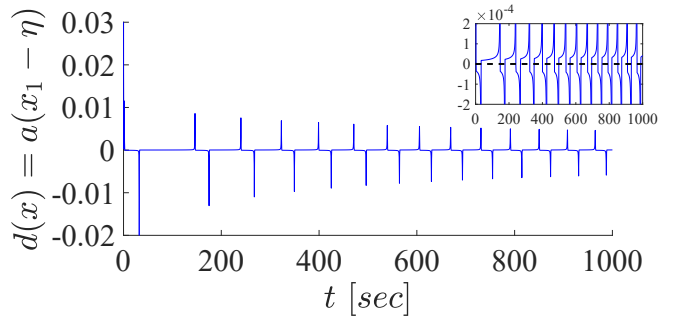

Fig. 6: Plot of the dither signal for $\mu = 0.3$. The magnified plot on the top right indicates that the dither $d(x) \neq 0$, though spikes occur when the dither changes sign.
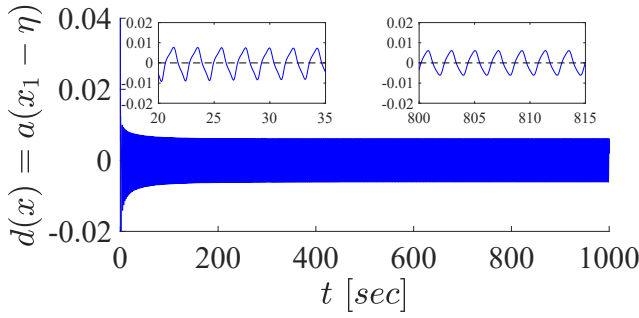
Fig. 7: Plot of the dither signal for $\mu = 3$. The magnified plots from $t = 20 - 35$ seconds and from $t = 800 - 815$ seconds are shown on the top left and top right, respectively.

frequency of the state-based dither is lower at $\mu = 0.3$ than those at $\mu = 3$. This is the benefit of using a time-invariant ESC, which automatically scales the dither signal parameters depending on the plant's speed.

Remark 3: *The convergence rate of the time-invariant ESC is comparable to the time-based ESC for $\mu = 1$. For slow plant speeds ($\mu = 0.3$), the time-based ESC fails to converge. The time-invariant ESC works for $\mu = 0.3$, but takes much longer to converge. The slow convergence rate of the time-invariant ESC can be attributed to the slow dither signal, $d(x)$, whose period of oscillation is about 150 seconds (see Fig. 6).*

V. CONCLUSIONS

In this paper, we proposed a time-invariant ESC for a periodic system, where we treat a periodic system state as the dither signal of the time-invariant ESC. The advantage of the proposed time-invariant ESC over the conventional time-based ESC is that, using the same ESC parameters, online optimization can be achieved for very slow systems that would normally violate the time-scale separation assumption. A secondary advantage of our proposed ESC scheme is that the convergence speed is faster for fast-frequency systems. On the other hand, the disadvantage is that for moderately slow systems it has a slower convergence rate. We presented a stability analysis of the time-invariant ESC scheme for a scalar case using averaging and singular perturbation tools. The simulations verified that the time-based ESC did not work well at slow speeds, but the time-invariant ESC succeeded. At faster plant speeds, the time-invariant ESC converged faster than the time-based ESC. However, our stability analysis did not explicitly show the effect of the operating speed of the plant on the convergence rate, which we aim to address in our future research. Finally, we would like to extend the current work for general classes of oscillators that require simultaneous adaptation of multiple parameters, which arise in applications such as control of powered prosthetic legs [22].

REFERENCES

[1] J. Buchli, L. Righetti, and A. J. Ijspeert, "Engineering entrainment and adaptation in limit cycle systems," *Biological Cybernetics*, vol. 95, no. 6, p. 645, 2006.

[2] M. Krstić and H.-H. Wang, "Stability of extremum seeking feedback for general nonlinear dynamic systems," *Automatica*, vol. 36, no. 4, pp. 595–601, 2000.

[3] K. B. Ariyur and M. Krstic, *Real-time optimization by extremum-seeking control*. John Wiley & Sons, 2003.

[4] H. H. Wang and M. Krstić, "Extremum seeking for limit cycle minimization," *IEEE Transactions on Automatic Control*, vol. 45, no. 12, pp. 2432–2437, 2000.

[5] M. Haring, N. Van De Wouw, and D. Nešić, "Extremum-seeking control for nonlinear systems with periodic steady-state outputs," *Automatica*, vol. 49, no. 6, pp. 1883–1891, 2013.

[6] F. J. Diedrich and W. H. Warren Jr, "Why change gaits? dynamics of the walk-run transition." *Journal of Experimental Psychology: Human Perception and Performance*, vol. 21, no. 1, p. 183, 1995.

[7] ——, "The dynamics of gait transitions: Effects of grade and load," *Journal of motor behavior*, vol. 30, no. 1, pp. 60–78, 1998.

[8] D. Quintero, D. J. Villarreal, and R. D. Gregg, "Preliminary experiments with a unified controller for a powered knee-ankle prosthetic leg across walking speeds," in *IEEE/RSJ Int. Conf. Intell. Robot. Syst.*, 2016, pp. 5427–5433.

[9] D. Quintero, D. J. Villarreal, D. J. Lambert, S. Kapp, and R. D. Gregg, "Continuous-phase control of a powered knee-ankle prosthesis: Amputee experiments across speeds and inclines," *IEEE Transactions on Robotics*, vol. 34, no. 3, pp. 686–701, June 2018.

[10] M. Guay and T. Zhang, "Adaptive extremum seeking control of nonlinear dynamic systems with parametric uncertainties," *Automatica*, vol. 39, no. 7, pp. 1283–1293, 2003.

[11] J. P. Krieger and M. Krstic, "Extremum Seeking Based on Atmospheric Turbulence for Aircraft Endurance," *Journal of Guidance, Control, and Dynamics*, vol. 34, no. 6, pp. 1876–1885, 2011. [Online]. Available: http://arc.aiaa.org/doi/10.2514/1.53825

[12] ——, "Aircraft endurance maximization at medium mach numbers by extremum seeking," *Journal of Guidance, Control, and Dynamics*, vol. 36, no. 2, pp. 390–403, 2013.

[13] C. Centioli, F. Iannone, G. Mazza, M. Panella, S. Podda, A. Tuccillo, V. Vitale, L. Pangione, and L. Zaccarian, "Extremum seeking applied to the plasma control system of the frascati tokamak upgrade," in *Proceedings of the 44th IEEE Conference on Decision and Control*, Dec 2005, pp. 8227–8232.

[14] D. Carnevale, A. Astolfi, C. Centioli, S. Podda, V. Vitale, and L. Zaccarian, "A new extremum seeking technique and its application to maximize RF heating on FTU," *Fusion Engineering and Design*, vol. 84, no. 2-6, pp. 554–558, 2009.

[15] N. Ghods and M. Krstic, "Extremum seeking with very slow or drifting sensors," in *2009 American Control Conference*, June 2009, pp. 1946–1951.

[16] ——, "Source seeking with very slow or drifting sensors," *Journal of Dynamic Systems, Measurement, and Control*, vol. 133, no. 4, p. 044504, 2011.

[17] H. K. Khalil, "Nonlinear systems, 3rd ed." *New Jersey, Prentice Hall*, 2002.

[18] Y. Tan, D. Nešić, and I. Mareels, "On non-local stability properties of extremum seeking control," *Automatica*, vol. 42, no. 6, pp. 889–903, 2006.

[19] S. Kumar and N. Gans, "Extremum seeking control for multi-objective optimization problems," in *IEEE Conf. Dec. Contr.*, 2016, pp. 1112–1118.

[20] S. H. Strogatz, *Nonlinear dynamics and chaos: with applications to physics, biology, chemistry, and engineering*. CRC Press, 2018.

[21] F. Bourland, R. Haberman, and W. Kath, "Averaging methods for the phase shift of arbitrarily perturbed strongly nonlinear oscillators with an application to capture," *SIAM Journal on Applied Mathematics*, vol. 51, no. 4, pp. 1150–1167, 1991.

[22] S. Kumar, A. Mohammadi, N. Gans, and R. D. Gregg, "Automatic tuning of virtual constraint-based control algorithms for powered knee-ankle prostheses," in *IEEE Conf. on Control Tech. and App.*, Aug 2017, pp. 812–818.